Original Article

Immunomodulatory effect of dimethyloxallyl glycine/nanosilicates-loaded fibrous structure on periodontal bone remodeling

Zi-Qi Liu, Ling-Ling Shang, Shao-Hua Ge*

Department of Periodontology, School and Hospital of Stomatology, Cheeloo College of Medicine, Shandong University & Shandong Key Laboratory of Oral Tissue Regeneration & Shandong Engineering Laboratory for Dental Materials and Oral Tissue Regeneration, No. 44-1, Wenhua Road West, Jinan, Shandong, 250012, China

Abstract *Background/purpose:* Relieving immuno-inflammatory responses is the prerequisite step for treating periodontitis. The angiogenic small molecule, dimethyloxalylglycine (DMOG), and osteoinductive inorganic nanomaterial, nanosilicate (nSi) have a powerful effect on bone regeneration, whereas the roles in osteoimmunomodulation have not been totally uncovered. Our study aimed to explore the immunomodulatory effect of DMOG/nSi-loaded fibrous membranes on periodontal bone remodeling.
Materials and methods: The fibrous membranes were prepared by incorporating DMOG and nSi into poly (lactic-co-glycolic acid) (PLGA) with electrospinning. The morphology features, surface chemical property and biocompatibility of DMOG/nSi-PLGA fibrous membranes were characterized. Thereafter, the fibrous membranes were implanted into rat periodontal defects, bone remodeling potential and immunomodulatory effect were evaluated by micro-computed tomography (micro-CT), histological evaluation and immunohistochemical analysis.
Results: DMOG/nSi-PLGA membranes possessed favorable physicochemical properties and biocompatibility. After the fibrous membranes implanted into periodontal defects, DMOG/nSi-PLGA membranes could relieve immuno-inflammatory responses of the defects (reduction of inflammatory cell infiltration, CD40L and CD11b-positive cells), increased CD206-positive M2 macrophages, and eventually facilitated periodontal bone regeneration.
Conclusion: DMOG/nSi-PLGA fibrous membranes exert protective effects during periodontal bone defect repairing, and steer immune response towards bone regeneration. Consequently, DMOG/nSi-PLGA fibrous membranes may serve as a promising scaffold in periodontal tissue engineering.

* Corresponding author.
  E-mail address: shaohuage@sdu.edu.cn (S.-H. Ge).

Introduction

Periodontitis is an infection-driven chronic disease in which the host immune response is disturbed by key pathogens, causing damage to the cementum, periodontal ligament and alveolar bone. The immune homeostasis maintained by immune cells regulating immuno-inflammatory response can minimize periodontal tissue damage.[1] Following the control of local inflammation, regeneration of the destroyed periodontium, especially alveolar bone, is equally significant, which is a crucial challenge for periodontal therapy. In recent years, some synthetic micromolecules or nanomaterials have come into existence for biotechnological and biomedical applications. These bioactive substances possess many advantages, such as favorable biological effects, preferable stability, small doses requirement and low cost.[2] Therefore, it is meaningful to develop a small molecule/nanomaterial-based bioactive structure to regulate immuno-inflammatory response and promote periodontal bone regeneration.

Dimethyloxalylglycine (DMOG), pharmacological inhibitor of prolyl hydroxylases (PHDs), can indirectly activate hypoxia-inducible factor 1 (HIF-1), which can regulate gene expression to adapt hypoxia, including angiogenic-related genes.[3] Consequently, DMOG significantly contributed to wound repair and bone regeneration *in vivo* by enhanced vascularization.[4–7] DMOG, on the other hand, has been reported to play a protective role in the development of inflammatory diseases such as inflammatory bowel disease (IBD), osteoarthritis, and apical periodontitis.[8–10] Studies indicated that DMOG or PHD inhibition diminished the secretion of pro-inflammatory cytokines and alleviated the response of immuno-inflammation *via* skewing macrophages towards anti-inflammatory M2 phenotype.[11,12] In our previous study, DMOG relieved lipopolysaccharide (LPS)-induced inflammatory response in human gingival fibroblasts, indicating its potential in treating periodontal diseases.[13] However, *in vivo* immunomodulatory effect of DMOG on periodontal tissue regeneration has not been revealed. Thus, it is essential to clarify its roles in the early inflammatory stage of periodontal defect healing.

Nanosilicate (nSi, $Na_{0.7}^+$ $[(Mg_{5.5}Li_{0.3})Si_8O_{20}(OH)_4]_{0.7}^-$) consists of synthetic two-dimensional silicate nanoplatelets with disk-shaped geometry of 20–50 nm in diameter and 1–2 nm in height. In an aqueous solution, nSi could dissociate into nontoxic ionic products, Na^+, Mg^{2+}, $Si(OH)_4$ and Li^+, which were beneficial to tissue regeneration.[14,15] The osteogenic effect of nSi has been reported in various types of cell and ectopic bone regeneration.[14,16–20] However, its roles in *in situ* osteogenesis, especially periodontal bone regeneration, have rarely been reported. In addition to its favorable osteogenic potential, nSi has been confirmed to possess osteo-immunomodulatory properties, and induce macrophage M2 phenotypic switch in the presence of bone marrow mesenchymal stem cells (BMSCs) to improve bone repairing.[21] Additionally, the individual ions (Li^+, Mg^{2+}, and $Si(OH)_4$) within nSi were intimately linked to immunomodulation. For instance, Mg plays a pivotal role in the immune system, and Mg deficiency was accompanied by increased levels of proinflammatory cytokines (IL-6, TNF-alpha) and inflammatory cell recruitment.[22] Small amounts of Mg, doping on a titanium surface, promoted polarization of macrophages to anti-inflammatory and pro-tissue healing M2 phenotype.[23] The released orthosilicic acid from sodium silicate might be responsible for its immune stimulatory effects and mitochondria activation.[24] Consequently, it is meaningful to explore the immunomodulatory properties and regenerative potential of nSi in periodontal bone regeneration.

In our study, angiogenic DMOG and osteogenic nSi were combined to maximize periodontal bone regeneration since alveolar bone is highly vascularized tissue. Poly (lactic acid-co-glycolic acid) (PLGA) is a popular non-toxic polymer with excellent biodegradability, biocompatibility and drug delivery ability.[25] Accordingly, DMOG/nSi-loaded PLGA fibrous membranes were prepared to explore the immunomodulatory effects of this dual release system on periodontal bone regeneration. The physicochemical properties and cell compatibility were characterized. Subsequently, the fibrous membranes were transplanted into a rat periodontal bone defect model, and micro-computed tomography (micro-CT), histological assessment and immunohistochemical analysis were performed to evaluate immunomodulation and periodontal bone regeneration.

Materials and methods

Materials

Poly (D, L-lactide-co-glycolide) (LA:GA = 75:25, MW = 90,000) was purchased from Jinan Daigang Biomaterial Co., Ltd, Jinan, China. Nanosilicates (type: Laponite XLG) were supplied by Southern Clay Products, Gonzales, TX, USA.

Preparation of DMOG/nSi-PLGA fibrous membranes

Electrospinning technique was used to prepare DMOG/nSi-PLGA fibrous membranes. PLGA was dissolved in hexafluoroisopropanol (HFIP, Macklin, Shanghai, China) to obtain the 20% (w/v) PLGA solution. Afterwards, DMOG (MCE, Monmouth Junction, NJ, USA, 1% w/w of PLGA) and nSi (5% w/w of PLGA) were dispersed in PLGA solution to get homogeneous solutions by sonicating and stirring. The spinning solution was transferred to a 5 mL syringe with a metal needle. A voltage of 11–13 kV was applied to the metal needle, and the distance between the needle tip and the

aluminum foil-covered collector was 18 cm. The solution flow rate was 2.5 mL/h. The electrospinning process was carried out at room temperature and relative humidity of 50%. After electrospinning, the collected fibrous membranes were vacuum-dried for two weeks in a desiccator to wipe off the residual organic solvent. The same protocol was used to prepare different PLGA fibrous membranes with or without DMOG and nSi, which were named as PLGA, nSi-PLGA, DMOG-PLGA and DMOG/nSi-PLGA, respectively.

Physicochemical characterizations of the fibrous membranes

The morphology characteristics and structure were observed under an S-4800 scanning electron microscope (SEM, Hitachi, Tokyo, Japan). Chemical composition was evaluated by a Fourier transform infrared spectroscopy (Thermo Scientific, Waltham, MA, USA).

Cell culture and cytocompatibility assessment of the fibrous membranes

The study protocol was approved by the Medical Ethical Committee of School of Stomatology, Shandong University (Protocol Number: GR201801). Human periodontal ligament stem cells (PDLSCs) were acquired from the periodontal ligament of healthy premolars for orthodontics requirement from 3 teenagers (14—16 years, 2 teeth each person), and all participants signed informed consent forms. All the protocols were based on the guidelines of the Helsinki Declaration of 1975, as revised in 2013.

Periodontal ligament tissues were collected from the middle third of the root surface. The scraped tissues were digested with 3 mg/mL collagenase I (Sigma Aldrich, St Louis, MO, USA) and 4 mg/mL dispase II (Sigma Aldrich) for 40 min at 37 °C. After termination of the digestion, the single-cell suspension was transferred to a 25 cm^2 air-permeable flasks, and the cells were cultured with α-minimum essential medium (α-MEM, HyClone, Beijing, China) containing 20% fetal bovine serum (FBS, BioInd, Kibbutz, Israel) and 1% antibiotics (100 U/ml of penicillin, 100 mg/mL of streptomycin, Sigma Aldrich, St Louis, MO, USA) at 37 °C in a 5% CO$_2$ incubator. The culture medium was changed once every 3 days, and the cells were passaged with 0.25% Trypsin—EDTA (Solarbio, Beijing, China) solution until 80—90% confluent monolayer cells. The passaged PDLSCs were then cultivated with 10% FBS α-MEM containing 1% antibiotics. Cells at passages 4—6 were used for the follow-up experiments.

The fibrous membranes were cut into 15 mm diameter in a 24-well plate, and sterilized in 75% ethanol for 1 h, followed by ultraviolet (UV) irradiation for 3 h. After being washed thrice with PBS, the fibrous membranes were immersed in α-MEM overnight. Then, PDLSCs were seeded at a density of 2×10^4 cells/well onto tissue culture plate (TCP) and different membranes. After incubation for 72 h, the effect of the fibers on cell viability was detected by cell counting kit-8 (CCK-8, Dojindo Laboratories, Kumamoto, Japan) according to the manufacturer's instructions. Briefly, the culture medium of each well was replaced with α-MEM medium containing 10% CCK-8 reagent, and the cells

were incubated at 37 °C for another 2.5 h. The optical absorbance value was measured at 450 nm wavelength using a microplate reader (SPECTROstar Nano, BMG Labtech, Offenburg, Germany).

Rat periodontal defect model preparation

The animal experiment complied with the guide of the Care and Use of Laboratory Animals of the Chinese Science and Technology Ministry. The study was authorized by the Medical Ethics Committee of School of Stomatology, Shandong University, Jinan, China (Permit Number: GD201801). All animal surgical operation was carried out under pentobarbital sodium anesthesia (40 mg/kg body weight). Besides, all efforts were made to minimize the suffering of the animals. Sixty 8-week-old male Wistar rats (SPF, Biotechnology Co., Ltd, Beijing, China) were used in this study.

A mandibular buccal bone defect ($5 \times 4 \times 1$ mm^3 L $\times$ W $\times$ D) was prepared using a dental drill. The critical bone defect was located proximately 1 mm distal to the front of the mandible, and the coronal margin of the bone defect was 1 mm apical to the crest of the alveolar bone. The rats were randomly divided into five groups. Different membranes were implanted into the defects: (1) no treatment (negative control, NC), (2) PLGA, (3) nSi-PLGA, (4) DMOG-PLGA, and (5) DMOG/nSi-PLGA. Surgical procedures were performed as previously described.[26] In this present study, the rats were randomly divided into five groups. Each rat had one defect at a unilateral mandible (n = 6 defects in each group). At 1 and 2 weeks post-surgery, the rats were sacrificed by excessive pentobarbital anesthesia and fixed with 4% paraformaldehyde by cardiac perfusion. The mandibles of the rats were harvested for the following experiments.

Micro-computational tomography (micro-CT) analysis

A micro-CT (PerkinElmer, Baesweiler, Germany) was used to scan the specimens to assess periodontal bone regeneration, with the scan settings of voltage 90 kV, current 88 μA and voxel resolution 50 μm at 360°. CT vox and CT analysis software were applied to reconstruct the images for 3D visualization and analysis. The region of interest (ROI) was drawn from the first slice containing the defect and moved distally until the defect area of defect disappeared. Furtherly, the quantitative indexes, including the percentage of bone volume (bone volume/tissue volume, BV/TV), trabecular thickness (Tb.Th) and trabecular separation (Tb. Sp) were measured and calculated to evaluate periodontal bone regeneration.

Histological analysis

The fixed samples were decalcified with 10% disodium ethylenediaminetetraacetate acid (EDTA) for 1 month at 4 °C. Afterwards, the samples were dehydrated in a graded series of ethanol solutions. After vitrification by dimethyl benzene, the samples were embedded in paraffin to incise the transverse section (5 μm thickness) of the

osteochondral defect area. Hematoxylin and eosin (H&E) staining and immunohistochemical staining for CD11b (Abcam, Cambridge, UK), iNOS (Abcam), CD206 (Abcam) were performed to appraise bone remodeling and immune-inflammatory response in periodontal defects according to the manufacturer's protocols. CD40L-positive cells were detected with immunofluorescence staining (CD40L, Abcam), and cell nuclei were stained with 4′,6-diamidino-2-phenylindole (DAPI) (Solarbio). The specimens were observed under a microscope (Olympus BX53, Tokyo, Japan), and the images were captured by the camera and imaging software (Olympus cellSens Standard 1.17). The newly formed bone was quantitatively analyzed, and the number of CD11b-, iNOS-, CD206-and CD40L-positive cells were counted with the Image pro-plus 6.0 software (Media Cybernetics, Silver Spring, MD, USA).

Statistical analysis

Data were shown as mean ± standard deviation (SD). Differences between more than two experimental groups and NC group were analyzed by one-way ANOVA followed by the Tukey HSD comparison test, and variance between two groups was compared by two-way t-test with GraphPad Prism software (version 6, by MacKiev Software, Boston, MA, USA). $P < 0.05$ was considered statistically significant.

Results

Physicochemical characterization of the fibrous membranes

The surface morphology of the membranes was characterized by SEM (Fig. 1A and B). The fibrous membranes exhibited an interlaced fibrous structure. All of the fibers possessed uniform and smooth morphology without beads or broken strands, and the mean diameters were 1073 nm (PLGA membranes) and 1007 nm (DMOG/nSi-PLGA membranes), respectively (Fig. 1C and D). The diameter of DMOG/nSi-PLGA fibrous membranes decreased in comparison with PLGA fibers.

The characteristic functional groups and surface chemical properties of the fibrous membranes were confirmed by FTIR spectra analysis (Fig. 1E). The peaks at 2995 cm^{-1} and 2946 cm^{-1} corresponded to −CH$_3$ and −CH vibrations, respectively. The strong absorption peak at 1746 cm^{-1} was due to the carbonyl −C═O stretching vibration. A couple of peaks at around 1050−1250 cm^{-1} were attributed to the −C−O stretching vibrations of the ester group. Additionally, the peak at 1452 cm^{-1} was ascribed to −CH$_2$ bending vibration, and the peaks at 990 and 685 cm^{-1} belonged to the −CH bending vibrations.[27,28] The characteristic peaks of PLGA and DMOG/nSi-PLGA membranes were similar to those of the raw PLGA, meaning that the surface chemical properties are unaffected by the electrospinning process.

Cytocompatibility of the fibrous membranes

CCK-8 assay was performed to assess the cytocompatibility of the fibrous membranes (Fig. 1F). After cultivation on different membranes for 72 h, PDLSCs exhibited relatively high cell viability. By contrast, the number of cells on DMOG/nSi-PLGA membranes accounts for around 80% of the number of cells on TCP, and there was no significant difference among all the membranes. Therefore, DMOG/nSi-PLGA membranes were biocompatible and could be applied for the following experiments.

Effect of DMOG/nSi-PLGA fibrous membranes on inflammatory cell infiltration and periodontal bone regeneration

H&E staining was used to evaluate inflammatory cell infiltration and bone repair preliminarily (Fig. 2). At 1 week post-surgery, the defects of NC group and PLGA group were full of fibrous tissue with inflammatory cell infiltration, and there was no new bone in the defect. For the other groups, few new bone was observed in the bone defects, while the number of inflammatory cells reduced. By contrast, DMOG/nSi-PLGA group had fewer inflammatory cells in the defect ($P < 0.05$). At week two, there was still few bone in the defects of NC group and PLGA group, whereas a small amount of new bone was found on the edge of the defects in other groups. DMOG/nSi-PLGA groups obtained more new bones than other two groups with the single bioactive substance, and fewer inflammatory cells were found in this group ($P < 0.05$).

Effect of DMOG/nSi-PLGA fibrous membranes on responses of macrophages

As shown in Fig. 3, the effect of DMOG/nSi-PLGA fibrous membranes on responses of macrophages was evaluated by immunohistochemical staining for iNOS and CD206. At week one after surgery, more iNOS-positive cells were found in NC and PLGA groups than other groups ($P < 0.0001$), and the fewest iNOS-positive cells were observed in DMOG/nSi-PLGA group among all groups ($P < 0.05$). At week two, overall, iNOS-positive cells reduced compared with week one, whereas the number of iNOS-positive cells in DMOG/nSi-PLGA group was still fewer than other groups (Fig. 3A, $P < 0.01$). On the contrary, at week one, fewer CD206-positive cells were shown in NC and PLGA groups compared with the other groups, and higher numbers of CD206-positive cells were found in DMOG/nSi-PLGA group in comparison with DMOG-PLGA and nSi-PLGA groups ($P < 0.05$). At week two, the number of CD206-positive cells decreased in general compared with week one, though more CD206-positive cells were seen in DMOG/nSi-PLGA group (Fig. 3B, $P < 0.0001$).

Effect of DMOG/nSi-PLGA fibrous membranes on the expression of immune cell markers

To further evaluate the immunomodulatory effect of DMOG/nSi-PLGA fibrous membranes, the expression of tumor necrosis factor (TNF) ligand superfamily member, CD40L and myeloid cell integrin, CD11b were detected by immunofluorescent and immunohistochemical staining. The trend for CD40L expression was more evident at week one post-operation. NC and PLGA groups presented higher
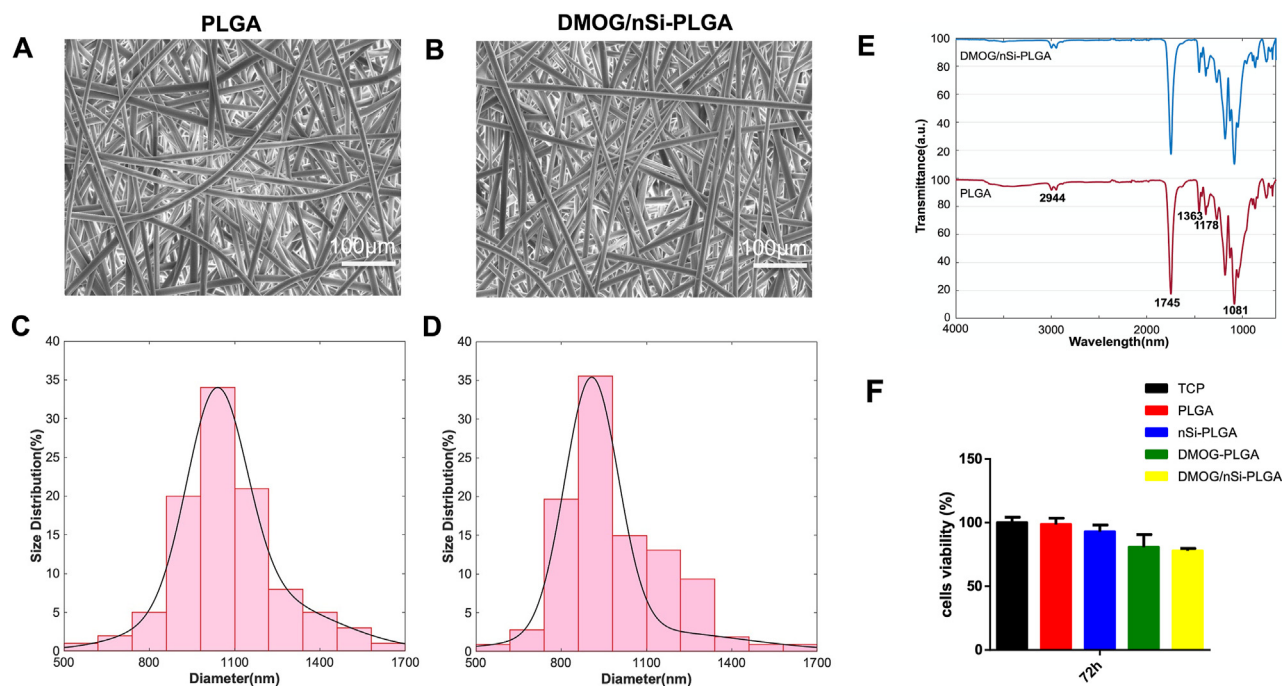
Figure 1 Characterization and cytocompatibility assessment of the fibrous membranes (A, B) SEM images of different fibrous membranes. Scale bar = 100 μm. (C, D) Diameter distribution analysis of different fibrous membranes. (A, C) PLGA (B, D) DMOG/nSi-PLGA. (E) FTIR spectra of the fibrous membranes. (F) Cell activity detected by CCK-8 assay after cultivation on TCP (tissue culture plate) and different fibrous membranes for 72 h. Data represent mean ± standard deviation (n = 3).

CD40L expression than the other groups. By contrast with DMOG-PLGA and nSi-PLGA groups, the number of CD40L-positive cells significantly reduced in DMOG/nSi-PLGA group (Fig. 4A, $P < 0.05$). Overall, at the second week, the expression of CD40L decreased significantly, while DMOG/nSi-PLGA group still exhibited the fewest CD40L-positive cells ($P < 0.01$). Analogously, CD11b expression in DMOG/nSi-PLGA group was the lowest among all groups at week one (Fig. 4B, $P < 0.01$). At week two, CD11b + cells were generally reduced in all groups, while the lowest expression was still observed in DMOG/nSi-PLGA group ($P < 0.01$).

Effect of DMOG/nSi-PLGA fibrous membranes on periodontal bone regeneration

Micro-CT was used to evaluate the effect of DMOG/nSi-PLGA fibrous membranes on periodontal bone repair. The specimens were scanned for mandibular bone remodeling analysis by micro-CT. The representative 3D digital reconstructed images indicated that a greater degree of bone healing and more newly formed calcified tissue were observed in DMOG/nSi-PLGA group than other groups. At week one, few newly formed bones were observed in NC and PLGA groups. At week two, the newly formed calcified tissue increased and the defect of DMOG/nSi-PLGA group was full of more new tissues (Fig. 5A). Quantitative analysis for the reconstructed images was further performed to characterize the new bone quantitatively and qualitatively with several indexes calculated from ROI. Consist with the 3D images, the percentage of bone volume (BV/TV) at week two was higher than that at week one, and DMOG/nSi-PLGA

group acquired the highest BV/TV level among all groups (Fig. 5B, $P < 0.001$), indicating that more new bones formed in this group. Additionally, the trabecular bone thickness (Tb.Th) of DMOG/nSi-PLGA group significantly augmented at week two (Fig. 5C, $P < 0.05$), and simultaneously, trabecular separation (Tb.Sp) reduced compared with the other groups at week two (Fig. 5D, $P < 0.05$), which suggested that the newly formed bones were much more mature and denser in DMOG/nSi-PLGA group. To some extent, DMOG-PLGA group also promoted bone repair, and nSi-PLGA group obtained more newly formed bones than NC and PLGA groups.

Discussion

In this study, we successfully prepared a DMOG/nSi-PLGA fibrous membranes for periodontal bone regeneration. The physicochemical properties and cell compatibility were characterized. After implantation *in vivo*, the immuno-modulatory effect of the fibrous structure during periodontal bone remodeling was evaluated by histomorphological assessment, immunohistochemical analysis and micro-CT.

The fibrous membranes were composed of interlaced fibers with smooth morphology and evenly distributed diameter. Compared with PLGA membranes, the diameter of DMOG/nSi-PLGA fibrous membranes decreased slightly, which may attribute to the increased electrical conductivity of spinning fluid by incorporation of nSi.[14,15] The FTIR spectra of PLGA and DMOG/nSi-PLGA membranes possessed similar characteristic peaks to those of the raw PLGA,
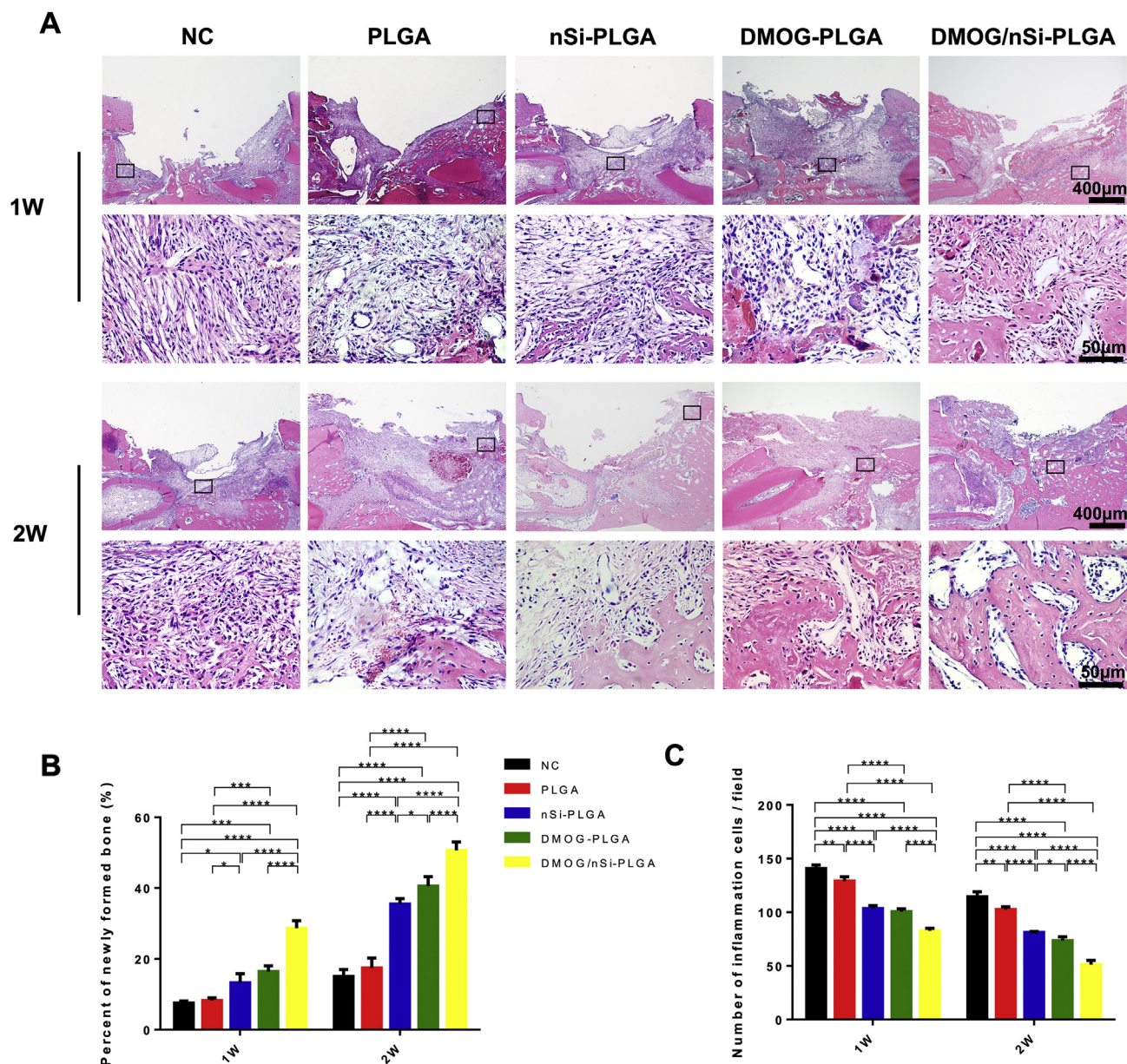
Figure 2 Histological analysis of tissue regeneration and inflammatory cell infiltration in five groups. (A) H&E staining of periodontal defect at 1 and 2 weeks post-surgery. The visual fields framed by the black line were magnified in the images below. (B) Quantitative analysis of newly formed bone areas in the five groups at two time points. (C) Quantitative analysis of number of inflammatory cells in new bone regeneration areas. Scale bar = 50 μm. Data represented mean ± standard deviation (n = 6). *P < 0.05, **P < 0.01, ***P < 0.001, ****P < 0.0001.

which suggested that the electrospinning process did not cause the change of the functional groups and surface chemical properties.[27,28] The unchanged surface chemical properties can avoid cell behavior being influenced by the diversity of surface properties.[29] DMOG and nSi were biocompatible and non-cytotoxic within a suitale concentration range,[13–15] and PLGA is a widely used polymer with superior biocompatibility.[30] After cultivation on different membranes for 72 h, CCK-8 assay indicated that PDLSCs still maintained high viability, which complied with the standard for cytocompatibility of biomaterials.[20] Consequently, the prepared PLGA-based membranes with or without

DMOG and nSi were cytocompatible and suitable for cell survival, which was consistent with a previous study.[31]

With the favorable biocompatibility, DMOG/nSi-PLGA fibrous membranes were implanted into a periodontal defect model of Wistar rats to evaluate the immunomodulatory effect of the fibrous membrane during periodontal bone repair. The immune homeostasis by immune cells regulating is crucial for wound healing and tissue regeneration. Tissue wound sites can recruit various immune cells, activate host defense reactions, and promote wound repair.[23] In recent years, macrophages have drawn extensive concerns as crucial regulators of tissue repair and
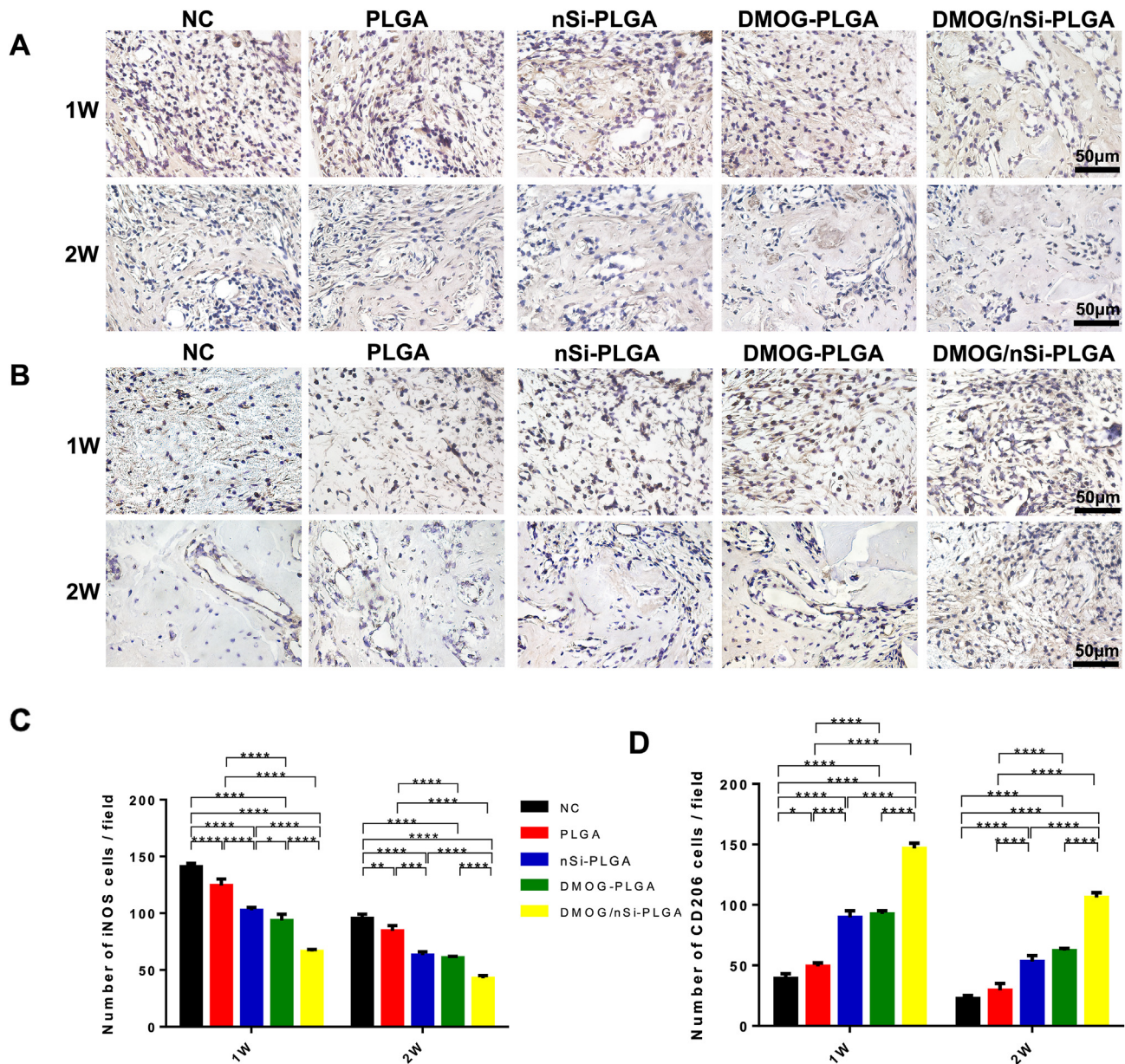
Figure 3 Immunohistochemical analysis of iNOS (A) and CD206 (B) expression level at 1 and 2 weeks post-surgery in five groups. (A) Immunochemical staining of iNOS. (B) Immunochemical staining of CD206. (C) Quantitative analysis of iNOS-positive cells. (D) Quantitative analysis of CD206-positive cells. Scale bar = 50 μm. Data represented mean ± standard deviation (n = 6). *P < 0.05, **P < 0.01, ***P < 0.001, ****P < 0.0001.

regeneration.[32] Following tissue injury, the phenotypes and functions of macrophages change in response to various environmental cues.[23,32] The "classically activated" pro-inflammatory M1 macrophages release inflammatory mediators such as interleukin (IL)-6, TNF-alpha, and inducible nitric oxide synthase (iNOS), and incur strong pro-inflammatory immune responses. Conversely, the "alternatively activated" anti-inflammatory M2 macrophages down-regulate inflammation and promote tissue repair by releasing anti-inflammatory cytokines, such as IL-4 and IL-10.[23,33] Consequently, it is beneficial to polarize the macrophages to the "alternatively activated" anti-inflammatory M2 phenotype for promoting tissue repair.

Macrophages exert multiple functions in different stages of inflammation and wound healing. In this present study, DMOG/nSi-PLGA fibrous membranes skewed macrophages towards the M2 phenotype at the early stage of tissue repairing. The results were supported by previous studies, indicating that DMOG and nSi could alleviate inflammation or improve tissue regeneration by modulating macrophage M2 phenotypic switch.[11,12,21] Therefore, DMOG/nSi-PLGA fibrous membranes had immunomodulatory effects on macrophage polarization during periodontal bone repair.

Interactions between B cell-expressed CD40, a TNF receptor superfamily member and its binding partner, CD40L, expressed by activated CD4+ T cells are known as co-
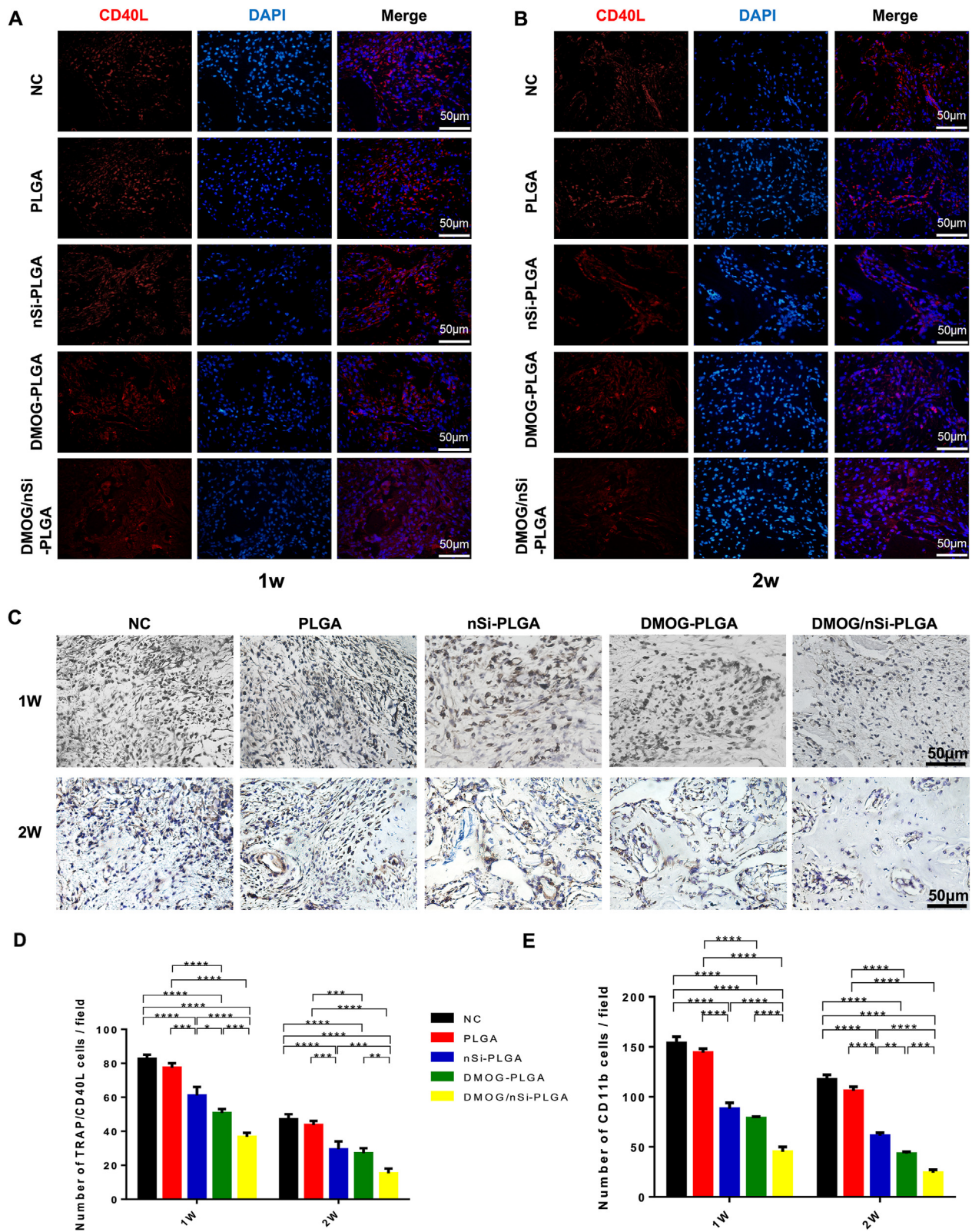
Figure 4 Expression of inflammatory factors at 1 and 2 weeks post-surgery in five groups. (A, B) Immunofluorescent staining of CD40L. Red indicated CD40L-positive cells. (C) Immunochemical staining of CD11b. (D) Quantitative analysis of CD40L-positive cells. (E) Quantitative analysis of CD11b-positive cells. Scale bar = 50 μm. Data represented mean ± standard deviation (n = 6). *P < 0.05, **P < 0.01, ***P < 0.001, ****P < 0.0001.
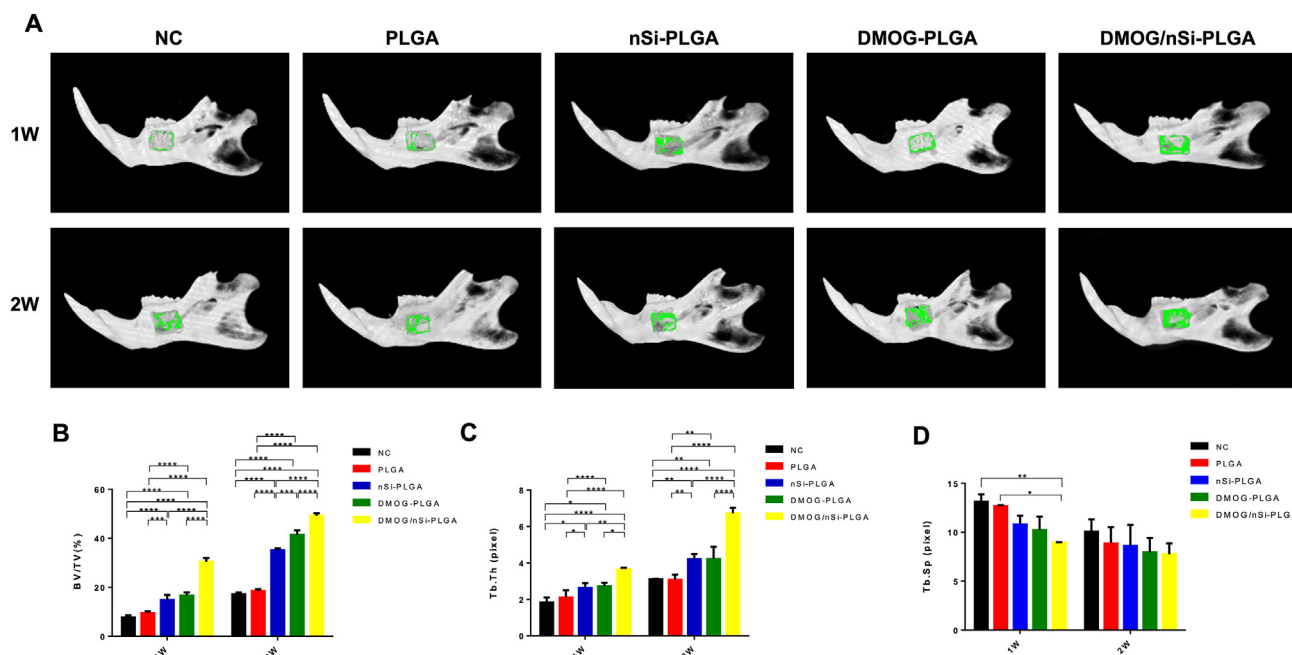
Figure 5 3D digital Micro-CT analysis of new bone regeneration at 1 and 2 weeks post-surgery in five groups. (A) Reconstructed 3D digital micro-CT images of mandibular bone defects. Green color presented repair area in mandibles after surgery. (B–D) Quantitative analysis of BV/TV, Tb. Th, and Tb. Sp by reconstruction and analysis software. Data represented mean ± standard deviation (n = 6). *$P < 0.05$, **$P < 0.01$, ***$P < 0.001$, ****$P < 0.0001$.

stimulatory molecules essential for germinal center formation.[34] In addition to immune cells, the CD40-CD40L axis also expressed on non-immune cells (e.g., endothelial cells, epithelial cells and fibroblasts) as well. It could trigger pro-inflammatory response and tissue damage, which was characterized by the release of inflammatory mediators such as matrix metalloproteinases (MMP), IL-1β, and TNF-alpha.[34–37] The expression of CD40L was down-regulated in DMOG/nSi-PLGA group at the early stages of tissue repair, suggesting that DMOG/nSi-PLGA fibrous membranes could relieve the immuno-inflammatory response by perturbing CD40-CD40L interaction and might reduce tissue damage.

Integrin CD11b, a member of the adhesion receptor family, is indispensable for inflammatory cell activation and migration to damaged tissues, thereby mediating inflammatory response. The decrease of the adhesion molecule CD11b on monocytes and granulocytes elicited an alleviation of inflammation in atrial fibrillation burden.[38] Additionally, CD11b has been reported to contribute to LPS-induced endotoxin shock and microbial sepsis, and CD11b activation promotes pro-inflammatory macrophage polarization.[39,40] Our study demonstrated that DMOG/nSi-PLGA group with the lowest expression of CD11b obtained the most effective tissue repair, which indicated that CD11b expression correlated positively with the inflammatory response in periodontal tissue damage.

The promotion effect of DMOG/nSi-PLGA fibrous membranes on bone regeneration was evaluated by micro-CT and H&E staining. Our study indicated that DMOG and nSi facilitated periodontal bone repair, respectively, whereas the combination of the two bioactive substances optimized the promotion effect. In addition to the intrinsic bioactive properties of DMOG and nSi, the beneficial immunomodulatory function contributed to the augmented regenerative potential of DMOG/nSi-PLGA fibrous membranes.

In this study, we successfully fabricated a DMOG/nSi-PLGA fibrous membrane for periodontal bone regeneration. The fibrous membranes were non-toxic and biocompatible, and supported cellular growth. After implanted into periodontal bone defects, DMOG/nSi-PLGA fibrous membranes exerted an immunomodulatory effect and relieved the inflammatory responses caused by tissue damage during periodontal bone repairing. Ultimately, the optimal periodontal bone regeneration was achieved with DMOG/nSi-PLGA implantation. However, the underlying mechanisms of the combined application of DMOG and nSi for enhanced periodontal bone regeneration remains to be elucidated. In conclusion, the combination of DMOG and nSi provides an effective strategy for periodontal inflammation control and tissue regeneration, and the fibrous membranes may be transformed into a prospective scaffold for periodontal regenerative medicine.

Declaration of competing interest

The authors declare that there is no conflict of interest.

Acknowledgements

References

1. Alvarez C, Rojas C, Rojas L, Cafferata EA, Monasterio G, Vernal R. Regulatory T lymphocytes in periodontitis: a translational view. *Mediat Inflamm* 2018;2018:7806912.

2. Woo KM, Jung HM, Oh JH, et al. Synergistic effects of dimethyloxalylglycine and butyrate incorporated into α-calcium sulfate on bone regeneration. *Biomaterials* 2015;39:1—14.

3. Semenza GL. Targeting hypoxia-inducible factor 1 to stimulate tissue vascularization. *J Invest Med* 2016;64:361—3.

4. Liang B, Liang J, Ding J, Xu J, Xu J, Chai Y. Dimethyloxaloylglycine-stimulated human bone marrow mesenchymal stem cell-derived exosomes enhance bone regeneration through angiogenesis by targeting the AKT/mTOR pathway. *Stem Cell Res Ther* 2019;10:335.

5. Zhang J, Guan J, Qi X, et al. Dimethyloxaloylglycine promotes the angiogenic activity of mesenchymal stem cells derived from iPSCs via activation of the PI3K/Akt pathway for bone regeneration. *Int J Biol Sci* 2016;12:639—52.

6. Zhang Q, Oh JH, Park CH, Baek JH, Ryoo HM, Woo KM. Effects of dimethyloxalylglycine-embedded Poly(ε-caprolactone) fiber meshes on wound healing in diabetic rats. *ACS Appl Mater Interfaces* 2017;9:7950—63.

7. Zhu M, Zhao S, Xin C, Zhu Y, Zhang C. 3D-printed dimethyloxallyl glycine delivery scaffolds to improve angiogenesis and osteogenesis. *Biomater Sci* 2015;3:1236—44.

8. Cummins EP, Seeballuck F, Keely SJ, et al. The hydroxylase inhibitor dimethyloxalylglycine is protective in a murine model of colitis. *Gastroenterology* 2008;134:156—65.

9. Hirai K, Furusho H, Hirota K, Sasaki H. Activation of hypoxia-inducible factor 1 attenuates periapical inflammation and bone loss. *Int J Oral Sci* 2018;10:12.

10. Hu S, Zhang C, Ni L, et al. Stabilization of HIF-1α alleviates osteoarthritis via enhancing mitophagy. *Cell Death Dis* 2020; 11:481.

11. Hams E, Saunders SP, Cummins EP, et al. The hydroxylase inhibitor dimethyloxallyl glycine attenuates endotoxic shock via alternative activation of macrophages and IL-10 production by B1 cells. *Shock* 2011;36:295—302.

12. Van Welden S, De Vos M, Wielockx B, et al. Haematopoietic prolyl hydroxylase-1 deficiency promotes M2 macrophage polarization and is both necessary and sufficient to protect against experimental colitis. *J Pathol* 2017;241:547—58.

13. Shang L, Wang T, Tong D, Kang W, Liang Q, Ge S. Prolyl hydroxylases positively regulated LPS-induced inflammation in human gingival fibroblasts via TLR4/MyD88-mediated AKT/NF-κB and MAPK pathways. *Cell Prolif* 2018;51:e12516.

14. Gaharwar AK, Cross LM, Peak CW, et al. 2D Nanoclay for biomedical applications: regenerative medicine, therapeutic delivery, and additive manufacturing. *Adv Mater* 2019;31: e1900332.

15. Tomás H, Alves CS, Rodrigues J. Laponite®: A key nanoplatform for biomedical applications? *Nanomedicine* 2018;14: 2407—20.

16. Carrow JK, Cross LM, Reese RW, et al. Widespread changes in transcriptome profile of human mesenchymal stem cells induced by two-dimensional nanosilicates. *Proc Natl Acad Sci U S A* 2018;115:E3905—13.

17. Cidonio G, Cooke M, Glinka M, Dawson JI, Grover L, Oreffo ROC. Printing bone in a gel: using nanocomposite bioink to print functionalised bone scaffolds. *Mater Today Bio* 2019;4:100028.

18. Gaharwar AK, Mihaila SM, Swami A, et al. Bioactive silicate nanoplatelets for osteogenic differentiation of human mesenchymal stem cells. *Adv Mater* 2013;25:3329—36.

19. Mihaila SM, Gaharwar AK, Reis RL, Khademhosseini A, Marques AP, Gomes ME. The osteogenic differentiation of SSEA-4 sub-population of human adipose derived stem cells using silicate nanoplatelets. *Biomaterials* 2014;35:9087—99.

20. Wang Y, Cui W, Chou J, Wen S, Sun Y, Zhang H. Electrospun nanosilicates-based organic/inorganic nanofibers for potential bone tissue engineering. *Colloids Surf B Biointerfaces* 2018; 172:90—7.

21. Li T, Liu Z, Xiao M, et al. Impact of bone marrow mesenchymal stem cell immunomodulation on the osteogenic effects of laponite. *Stem Cell Res Ther* 2018;9:100.

22. Tam M, Gómez S, González-Gross M, Marcos A. Possible roles of magnesium on the immune system. *Eur J Clin Nutr* 2003;57: 1193—7.

23. Li B, Cao H, Zhao Y, et al. In vitro and in vivo responses of macrophages to magnesium-doped titanium. *Sci Rep* 2017;7: 42707.

24. Jurkić LM, Cepanec I, Pavelić SK, Pavelić K. Biological and therapeutic effects of ortho-silicic acid and some ortho-silicic acid-releasing compounds: new perspectives for therapy. *Nutr Metab* 2013;10:2.

25. Mir M, Ahmed N, Rehman AU. Recent applications of PLGA based nanostructures in drug delivery. *Colloids Surf B Biointerfaces* 2017;159:217—31.

26. Wang F, Du L, Ge S. PTH/SDF-1α cotherapy induces CD90+CD34- stromal cells migration and promotes tissue regeneration in a rat periodontal defect model. *Sci Rep* 2016;6: 30403.

27. Kankala RK, Xu X, Liu C, Chen A, Wang S. 3D-Printing of microfibrous porous scaffolds based on hybrid approaches for bone tissue engineering. *Polymers* 2018;10:807.

28. Masaeli R, Jafarzadeh S, Kashi T, Dinarvand R, Tahriri M, Rakhshan V, Esfandyari-Manesh M. Preparation, characterization and evaluation of drug release properties of simvastatin-loaded PLGA microspheres. *Iran J Pharm Res (IJPR)* 2016;15: 205—11.

29. Ma B, Zhang S, Liu F, et al. One-dimensional hydroxyapatite nanostructures with tunable length for efficient stem cell differentiation regulation. *ACS Appl Mater Interfaces* 2017;9: 33717—27.

30. Kapoor DN, Bhatia A, Kaur R, Sharma R, Kaur G, Dhawan S. PLGA: a unique polymer for drug delivery. *Ther Deliv* 2015;6: 41—58.

31. Wang Z, Hu J, Yu J, Chen D. Preparation and characterization of Nano-Laponite/PLGA composite scaffolds for urethra tissue engineering. *Mol Biotechnol* 2020;62:192—9.

32. Wynn TA, Vannella KM. Macrophages in tissue repair, regeneration, and fibrosis. *Immunity* 2016;44:450—62.

33. Snyder RJ, Lantis J, Kirsner RS, Shah V, Molyneaux M, Carter MJ. Macrophages: a review of their role in wound healing and their therapeutic use. *Wound Repair Regen* 2016; 24:613—29.

34. Karnell JL, Rieder SA, Ettinger R, Kolbeck R. Targeting the CD40-CD40L pathway in autoimmune diseases: humoral immunity and beyond. *Adv Drug Deliv Rev* 2019;141:92—103.

35. Han L, Dai L, Zhao Y, et al. Correction: CD40L promotes development of acute aortic dissection via induction of inflammation and impairment of endothelial cell function. *Aging* 2018;10:3627.

36. Lievens D, Eijgelaar WJ, Biessen EA, Daemen MJ, Lutgens E. The multi-functionality of CD40L and its receptor CD40 in atherosclerosis. *Thromb Haemostasis* 2009;102:206—14.

37. Román-Fernández IV, García-Chagollán M, Cerpa-Cruz S, et al. Assessment of CD40 and CD40L expression in rheumatoid arthritis patients, association with clinical features and DAS28. *Clin Exp Med* 2019;19:427—37.

38. Tarnowski D, Plichta L, Forkmann M, et al. Reduction of atrial fibrillation burden by pulmonary vein isolation leads to a decrease of CD11b expression on inflammatory cells. *Europace* 2018;20:459—65.

39. Schmid MC, Khan SQ, Kaneda MM, et al. Integrin CD11b activation drives anti-tumor innate immunity. *Nat Commun* 2018; 9:5379.

40. Zhou H, Li Y, Gui H, et al. Antagonism of Integrin CD11b affords protection against endotoxin shock and polymicrobial sepsis via attenuation of HMGB1 nucleocytoplasmic translocation and extracellular release. *J Immunol* 2018;200:1771—80.